An Enzyme Cascade with Horseradish Peroxidase Readout for High-throughput Screening and Engineering of Human Arginase-1

Jaime Fernández de Santaella[‡, 1, 2,3], Jin Ren[‡, 1, 2], Rosario Vanella[1, 2], Michael A. Nash[1, 2, 3, 4] *

[1] Institute of Physical Chemistry, Department of Chemistry, University of Basel, 4058 Basel, Switzerland
[2] Department of Biosystems Science and Engineering, ETH Zurich, 4058 Basel, Switzerland
[3] National Center for Competence in Research (NCCR), Molecular Systems Engineering, 4058 Basel, Switzerland
[4] Swiss Nanoscience Institute, 4056 Basel, Switzerland

‡ Equally contributing
* Corresponding author: michael.nash@unibas.ch

Abstract

We report an enzyme cascade with horseradish peroxidase-based readout for screening human arginase-1 (hArg1) activity. We combined the four enzymes hArg1, ornithine decarboxylase, putrescine oxidase and horseradish peroxidase in a reaction cascade that generated colorimetric or fluorescent signals in response to hArg1 activity and used this cascade to assay wild type and variant hArg1 sequences as soluble enzymes and displayed on the surface of *E. coli*. We screened a curated 13-member hArg1 library covering mutations that modified the electrostatic environment surrounding catalytic residues D128 and H141, and identified the R21E variant with 13% enhanced catalytic turnover rate compared to wild type. Our scalable one-pot single-step arginase assay with continuous kinetic readout is amenable to high-throughput screening and directed evolution of arginase libraries, and testing drug candidates for arginase inhibition.

Table of Contents – Graphical abstract

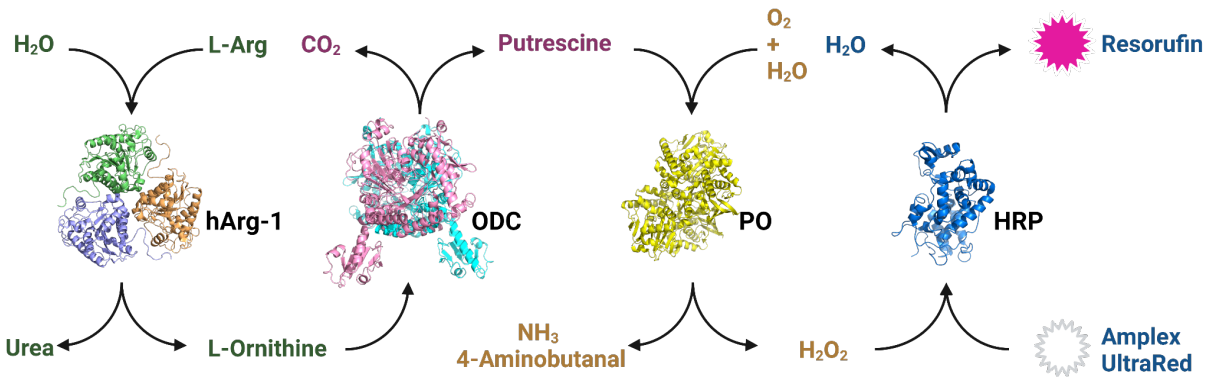

Introduction

Arginase is a stereoselective hydrolase found in bacteria and eukarya that plays a key role in human health and metabolism. Arginase catalyzes the hydrolysis of L-arginine into L-ornithine and urea and is expressed in at least two known isoforms in humans (hArg1 and hArg2). Human arginase 1 (hArg1) is a cytosolic isoform predominantly expressed in the liver that regulates ureagenesis, while hArg2 is a mitochondrial isoform found primarily in the intestines, kidneys and prostate.[1] hArg1 is a homotrimeric metalloenzyme, 322 residues in length with each monomer coordinating a binuclear Mn^{2+}-cluster bridged by a hydroxide ion inside its catalytic core in an α/β-fold. The mechanism of the reaction has been proposed based on high resolution x-ray crystal structures with different substrates and inhibitors.[2–5]

Both hArg1 and hArg2 are relevant drug targets for inhibition by small molecules, having been implicated in over 30 severe medical conditions[5] from severe cardiovascular disease[6] to several cancers,[7–9] and rare metabolic diseases.[10] Arginase has further been proposed as a therapeutic enzyme for treating argininemia, a rare recessive autosomal disorder caused by arginase dysfunction.[11,12] Metabolic therapy for treatment of hepatocellular carcinomas and melanomas is another potential application area for hArg1. These cancers are deficient in argininosuccinate synthetase 1 or ornithine transcarbamylase, which are responsible for arginine synthesis, rendering them auxotrophic for extracellular L-arginine.[1] As a result, L-arginine depletion by hArg1-treatment is currently under investigation for depletion of blood arginine levels thereby starving cancer cells of an essential substrate.[13–17]

These biomedical applications have generated a need for rapid and sensitive arginase activity assays. Existing arginase assays include schemes for derivatization and detection of urea. For example, diacetyl monoxime-urea and o-phthalaldehyde-NED reactions to derivatize urea into a colorimetric dye.[18,19] This assay requires multi-step reactions under acidic conditions and elevated temperatures, is not easily scalable and provides an endpoint only. Urease-based methods rely on enzymatic conversion of urea to ammonia, which is then either converted by a subsequent reaction to a colorimetric reagent such as indophenol[20] or read out using electrochemical sensing.[21,22] A limitation of the urease approach is that the specificity of urease-dependent assays is low for biological samples containing high ammonia backgrounds. Inactivation, inhibition or suboptimal activity of urease, particularly when immobilized on an electrode surface can further present challenges. Arginase activity can also be measured from derivatized ornithine. However, this method also requires sample treatment under harsh conditions and is limited to endpoint kinetics.[23] Mass spectroscopy-based arginase activity assays have been reported, relying on hydrophilic interaction chromatography combined with RapidFire[24] or self-assembled monolayer desorption ionization (SAMDI),[25] however these assays require large infrastructure and rely on multi-step chromatographic separation and derivatization steps. Recently, Grobben et al.[26] developed a fluorescent dye that was quenched by L-ornithine, resulting in fluorescence enhancement when the enzyme was inhibited. This straightforward assay allowed for real time monitoring of the reaction progress, however, high signal-to-noise and autofluorescence resulted in a high false positive rate (64%) and a low Z factor (0.59). Currently available arginase activity assays are therefore limited in terms of ease of use, throughput, sensitivity, and time resolution. These limitations currently hinder our ability to engineer hArg1 efficiently and screen small molecule arginase inhibitors.

Here we report a novel enzyme cascade assay that converts the arginase reaction product L-ornithine into hydrogen peroxide and uses horseradish peroxidase (HRP) to generate signal (**Scheme**

1). This one-pot single-step assay continuously generates a colorimetric or fluorescent signal, is compatible with a broad range of HRP substrates, and allows straightforward fitting of enzyme parameters K_m and k_{cat} without the need for performing endpoint measurements at different time points.[27] Efficient enzymatic reaction cascade design prevents rate-limiting reactions and intermediate accumulation while providing alternative chemical routes and signal amplification.[28–32] Additionally, bacterial cell-surface display of active hArg1 was achieved and used to validate the assay. We used this assay to screen a small curated library of 13 hArg1 variants, and detected small differences in K_M and k_{cat}. The mutant library was analyzed successfully and showed good concordance for both *E. coli* surface-displayed and soluble hArg1 variants.

Experimental section

Chemicals, materials and protein synthesis

Standard procedures were followed for the purchasing and protein purification. For more detail see the Supplementary Information.

Colorimetric activity assay of soluble hArg1

Prior to the experiment, hArg1 samples were incubated with $MnCl_2$ at a 2 molar-ratio excess at room temperature for 20 mins. Assay components were dissolved in HEPES buffer (pH 7.4) and all but the substrate were premixed and added simultaneously to a 96-well plate pre-loaded with the substrate L-arginine. Unless otherwise stated, the final concentrations were 5 nM hArg1 WT or variant, 1 µM ODC, 500 nM PO, 50 nM HRP, 100 µM Amplex UltraRed in 100 µL HEPES buffer (pH 7.4). The pH range was determined in HEPES buffer that was premixed with the basic substrate and adjusted to the final pH with HCl and NaOH. The absorbance for each well was measured continuously at 570 nm for 30 minutes at 37 °C with a Tecan Safire 2 microplate reader.

***E. coli* surface display**

hArg1 gene was cloned into the N-terminus of an AIDA-1 autotransporter anchor protein flanked by a 6x-His-Tag. The plasmid was transformed into NiCo21 competent *E. coli* cells. Enzyme surface-display was achieved after inducing at an OD_{600} = 0.6 with a final concentration 0.5 mM IPTG and incubating at 37 °C for 24 hours. Successful display of the construct was validated by two-step immunofluorescence labeling (primary anti-His labeling and secondary anti-IgG fluorescent antibody) and verified with flow cytometry.

Fluorescence activity assay of *E. coli*-displayed hArg1

All components of the assay were pre-dissolved in PBS buffer (pH 7.4) and all but the substrate were premixed and added simultaneously to a black 96-well plate pre-loaded with the substrate L-arginine. Unless otherwise stated, the final concentrations of all components were 5 million cells/mL, 1 µM ODC, 500 nM PO, 50 nM HRP, 100 µM Amplex UltraRed in 100 µL PBS buffer (pH 7.4), where cell density was estimated from the OD_{600}. The fluorescence signal (Ex. 530 nm; Em. 590 nm) was measured continuously for 30 minutes at 37 °C with a Safire 2 Tecan plate reader in triplicate. The reaction rate was then normalized according to the expression level of each sample and a Michaelis-Menten fit was used to estimate the kinetic parameters.

Differential Scanning Fluorimetry (NanoDSF)

A Prometheus NT.48 instrument (NanoTemper Technologies) was used to characterize the thermal denaturation temperatures of human arginase variants following standard protocols. For more detail see the Supporting Information.

Results and Discussion

Colorimetric enzyme cascade assay

Our kinetic assay consists of a one-pot single-step mix and run enzyme cascade comprising hArg1, ODC, PO, and HRP (**Scheme 1**). hArg1 hydrolyses L-arginine to produce urea and L-ornithine. The first intermediate L-ornithine is cleaved by ODC to form CO_2 and putrescine, which is then further oxidized by PO to 4-aminobutanal and H_2O_2. Finally, HRP uses H_2O_2 to oxidize the substrate Amplex UltraRed into resorufin, generating a fluorescent product detectable in either absorbance (ε_{max} at 570 nm) or fluorescence (Ex./Em. 530/590 nm) mode. The cascade maintains a 1:1 stoichiometry between L-arginine hydrolysis and resorufin production, simplifying calibration and quantification of enzyme kinetic parameters with this approach. To calibrate the assay, we first generated an Amplex UltraRed/resorufin standard curve which maintained a linear relationship between absorbance and H_2O_2 concentration between 0 - 100 µM H_2O_2 converted by 100 nM of HRP (**Figure 1a**).

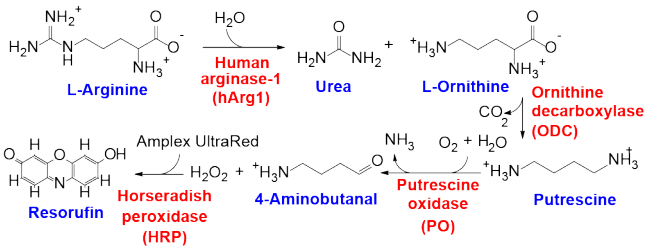

Scheme 1: Enzyme cascade for assaying hArg1 activity.

To validate the assay design, we cloned, expressed and purified hArg1, ODC and PO from *E. coli*, and obtained HRP commercially. Primary amino acid sequences of hArg1, ODC and PO are provided in the Supplementary information. The sizes and purity of *E. coli* expressed enzymes were confirmed by size exclusion chromatography and SDS-PAGE (**Supplementary Figure 1**). We explored the reaction conditions by first testing a range of concentrations of the downstream auxiliary enzymes (ODC, PO and HRP) to ensure that the hArg1 reaction was the rate limiting step of the overall cascade. We set the hArg1 concentration relatively low (5 nM) and titrated the concentrations of each of the auxiliary enzymes while maintaining excess of all other auxiliary enzymes. As shown in **Supplementary Figure 2**, the three auxiliary enzymes show rate-limiting effects at low concentrations, which disappear at sufficiently high excess (50-, 30-, and 0.32-fold molar excess with respect to hArg1 set at a concentration of 5 nM). In the absence of any one of the auxiliary enzymes, the cascade generated little to no signal. Under our typical assay conditions, we set ODC, PO and HRP at 200-, 100- and 10-fold molar excess to 5 nM hArg1. Under these excess conditions of auxiliary enzymes, the reaction step catalyzed by hArg1 is rate-limiting for the overall cascade.

We observed a lag phase in reaction velocity at early time points before the cascade reached a steady state (**Figure 1b**). Such non-linearities are common for cascade reactions.[30] However, the presence of the lag phase may affect the precision of determining the enzyme kinetic parameters, since the initial rate of the reaction will be underestimated. We tested a range of hArg1 concentrations and performed linear fitting of reaction velocity from 600-1200 s, which represented a time window after the system reached steady state. When varying the concentration of hArg1, we found the initial reaction velocity to be linear from 0-5 nM (**Figure 1c**). Since the previously reported pH optimum for hArg1 activity is 9.5,[4] we studied the effect of pH on the assay and its functionality at pH 9.5. As a whole, the cascade retained more than 80% of activity between physiological pH and pH 10.5, with the highest activity recorded at pH 9.3 (**Figure 1d**). The activity of each member of the cascade was

retained between pH 5.5 and 9.5 (**Supplementary Figure 3**). To ensure hArg1 was still acting as the rate-limiting step at a higher pH, the molar excess of ODC, PO and HRP was increased to 5000-, 1000- and 500-fold, respectively.

To measure Michaelis–Menten parameters for hArg1 we varied the L-arginine substrate concentration across a range from 0.5-20 mM and measured the reaction velocity using the full cascade (**Figure 1e**). The resulting fit generated parameter values of K_M = 1.16 ± 0.02 mM and k_{cat} = 16 ± 0.5 s^{-1} (**Figure 1f**) for hArg1 at pH 7.4. This K_M value was consistent with values reported in the literature using various methodologies, whereas the k_{cat} value, which historically has a wider range of reported values, was lower than previous reports (**Supplementary Table 1**). The wide range of reported k_{cat} values in the literature could be attributable to varying levels of purity in hArg1 preparations from various labs, or differences in protein constructs (e.g., affinity tags). We also used a commercially available arginase assay kit from Sigma-Aldrich (product number MAK112) to measure the kinetic parameters of our hArg1 preparation (**Supplementary Figure 4**), and found k_{cat} = 26 ±1.3 s^{-1} and K_M = 1.65 ± 0.14 mM, which were comparable to the parameters obtained with our cascade system.

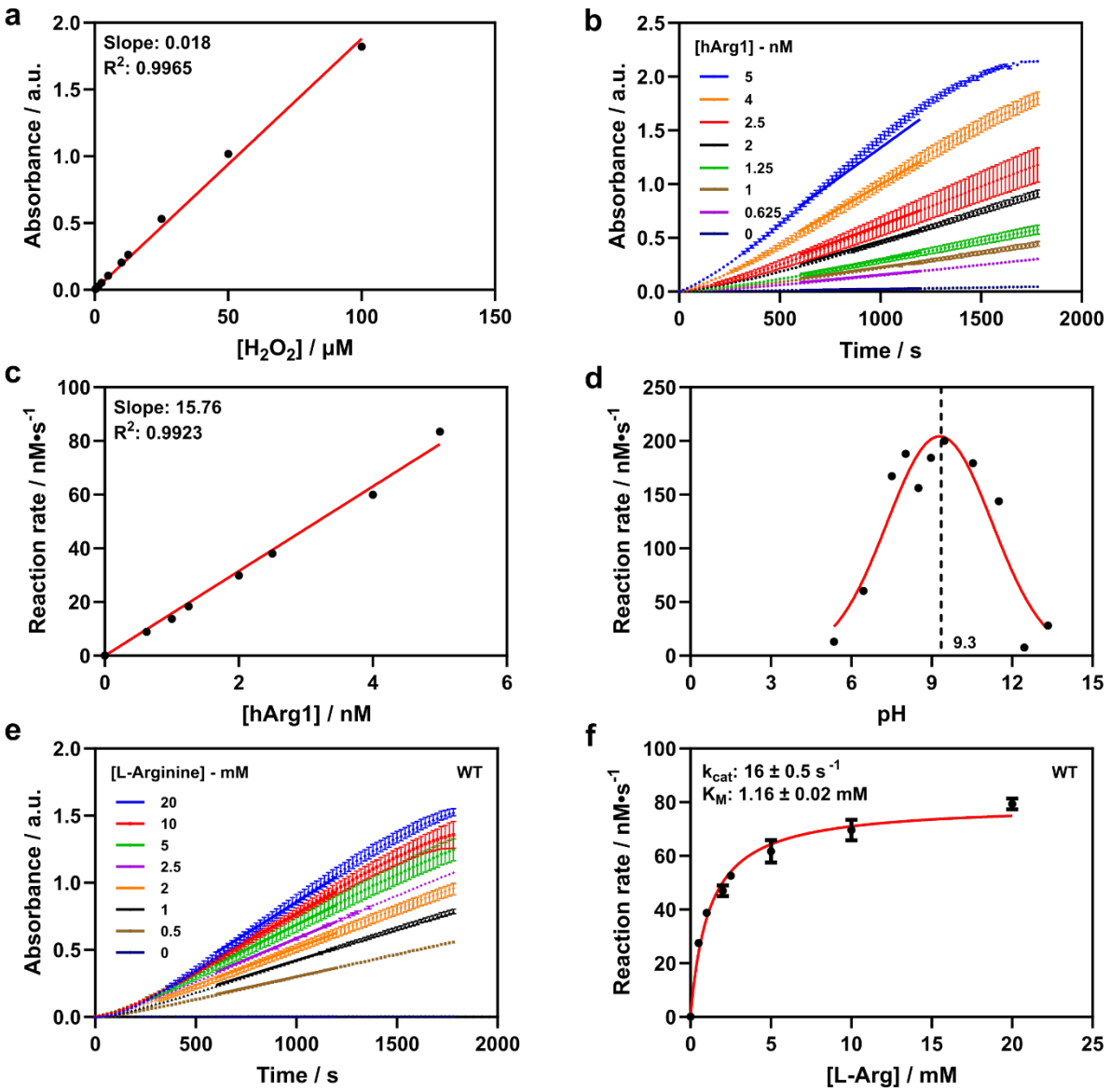

Figure 1: Characterization and validation of the enzyme cascade assay. (a) Standard curve showing absorbance of Amplex Ultrared for different concentrations of H_2O_2 ([HRP]= 100 nM, time= 160 s). **(b)** Time-course experiment at various concentrations of hArg1 showing a detectable lag phase (0 - 600 s). Linear regression used for calculating reaction rate was obtained from data points between 600 - 1200 seconds and is represented by a solid line. **(c)** Determination of the linear range for soluble hArg1 with the full cascade. **(d)** Determination of valid pH range for the hArg1 activity assay with the full cascade. The estimated pH of maximal activity is shown as a blackline. **(e)** Time course of 5 nM hArg1 WT with varying substrate concentration (0-20 mM) used for K_M and k_{cat} fitting. The linear regression (600-1200 s) is represented by a solid line. **(f)** Michaelis-Menten fit of the WT hArg1 to estimate kinetic parameters. hArg1 WT and variants were activated by Mn^{2+}. Data points represent the mean and SD as error bars (n=3). All measurements were performed at pH 7.4 in HEPES buffer except the data in panel (d).

Design of a hArg1 curated library

We next designed a small mutational library with charged residues near the catalytic center to demonstrate the value of the cascade assay in facile screening of hArg1 variants. We hypothesized that a mutational library targeting electrostatic interactions and influencing the ionization state of H141 and D128 could potentially generate valuable and insightful mutants. Di Constanzo et al. (2010)[2] proposed that the first and second-shell residues D128 and H141 act as a proton shuttle and proton donor at the catalytic center of hArg1, respectively. Since the natural pH optimum for hArg1 activity is 9.5,[4] at physiological pH the electrostatic environments of these two residues could be suboptimal for these purposes. More specifically, H141 has a dual function in the catalytic center: (1) the initial and possibly the rate-limiting step of the reaction is the formation of a hydroxide ion, which is supposedly mediated by H141 by capturing the free proton, via a solvent molecule. (2) H141 donates a proton to the L-ornithine leaving amino group. At physiological pH, we hypothesize that a more negatively-charged microenvironment could promote H141 protonation and impact hArg1 activity. On the other hand, D128 coordinates one of the Mn^{2+} ions and donates a proton to the product L-ornithine. We hypothesized that creating a positively-charged microenvironment for D128 would have an impact on the rate of product release. As a result, 13 single mutants were chosen: G18D/E, E277D, Q19E/D, T246E/D, and R21E/D within 4 Å of H141 and V145R/K and E186R/K within 5 Å of D128 (**Figure 2**).

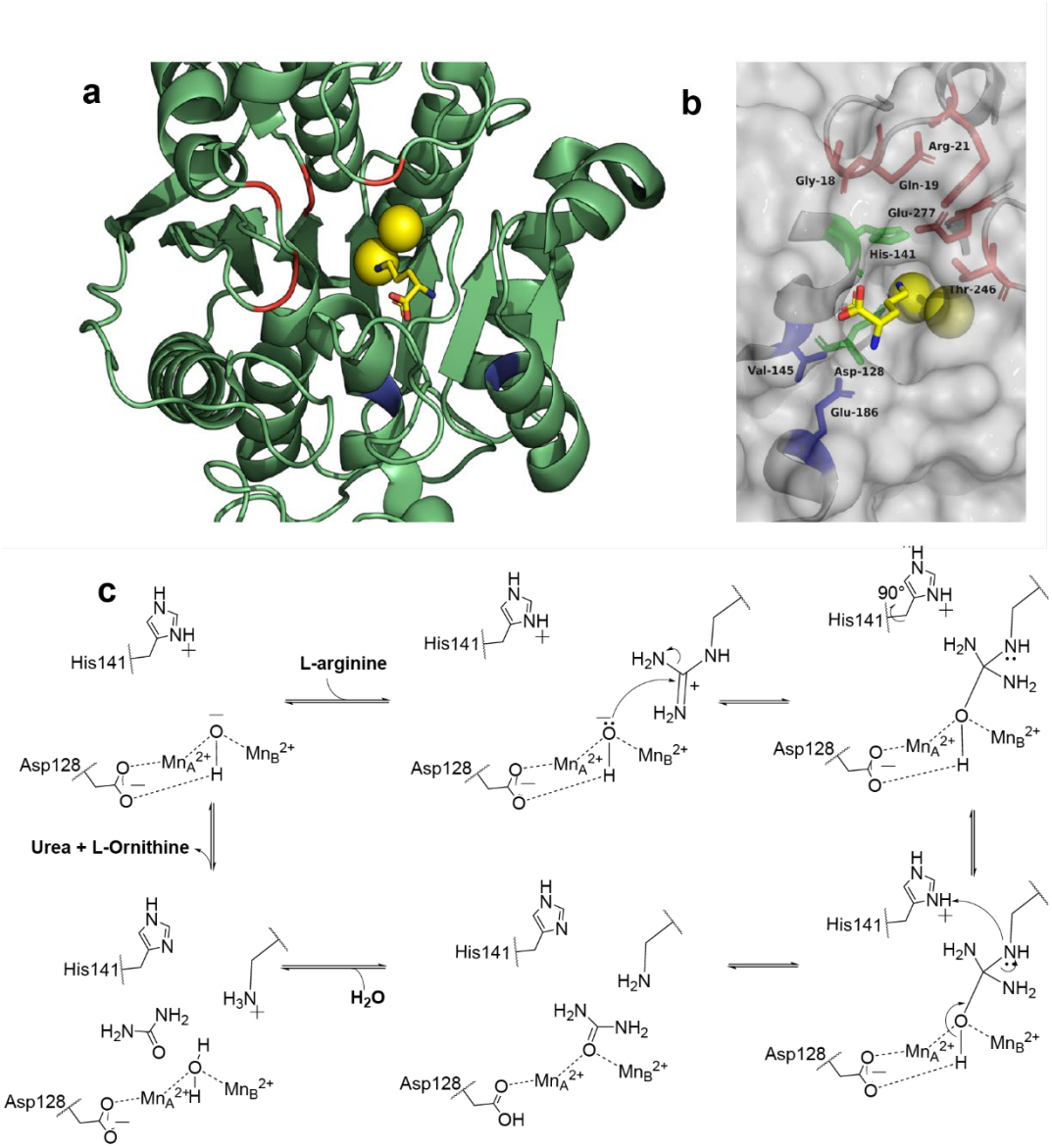

Figure 2: Design of the curated mutational library. (a) Crystal structure of hArg1 monomer (from PDB: 3GMZ)[36] in complex with L-ornithine. Mutational spots near H141 and D128 highlighted in red and blue, respectively. The binuclear Mn^{2+}-cluster is also shown as yellow spheres and L-ornithine as a yellow stick. **(b)** Crystal structure of hArg1 monomer with a stick representation of the active site proximal to the binuclear Mn^{2+}-cluster with the mutational targets represented in the same color scheme as panel (a). H141 and D128 are shown in green. The surface of the monomer is represented in dark gray. **(c)** Proposed roles of H141 and D128 in the catalytic mechanism hArg1. H141 acts as a proton shuttle, while D128 may act as a proton donor before the product release. Figure modified from previous literature.[2,37]

Kinetic characterization of hArg1 variant library

Genes encoding all variant hArg1 sequences in the curated library were synthesized, cloned into pET28a vectors, expressed and purified in *E. coli* with comparable yields to WT. Subsequently, these mutants were classified as active or inactive in a preliminary screen: an absorbance time-course assay under substrate-saturated conditions (20 mM of L-arginine) and the previously established optimal conditions of the cascade (5 nM of each variant, 1 µM of ODC, 500 nM of PO and 50 nM of HRP) (**Figure**

3a-b). Three out of nine variants encoding single point mutations around H141 significantly lost their catalytic function while two variants retained ~10 % of the WT activity level. Another three mutants exhibited a reduction in the turnover number (between 75% and 52% of the WT) and one mutant (R21E) showed slightly better performance than WT. The K_M values were not significantly impacted, which was in agreement with H141 not being involved in the substrate binding (**Supplementary Table 2** and **Figure 2c**).[38] Finally, we titrated the L-arginine substrate concentration (**Figure 3c** and **Supplementary Figure 5**) and measured reaction rates from t=600-1200 s to obtain a Michaelis-Menten fit and extract K_M and k_{cat} for the variants (**Figure 3c** and **Supplementary Table 2**).

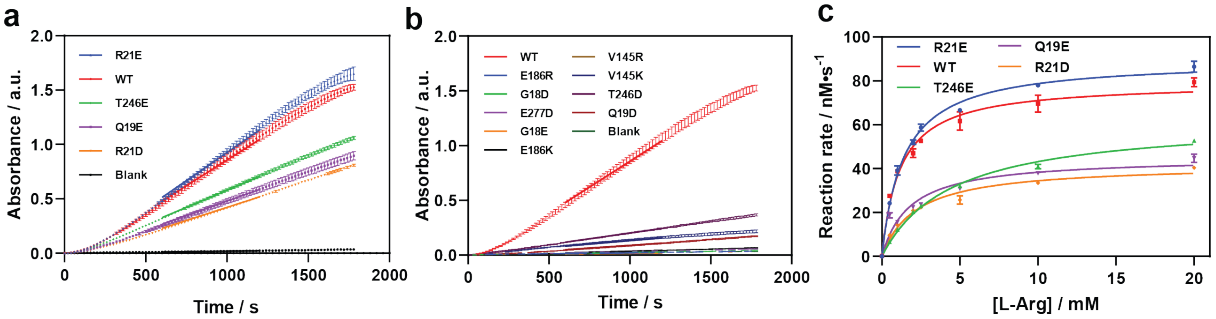

Figure 3: Screening of the rational-designed library. Time course of 5 nM hArg1 WT and all the synthesized variants with 20 mM L-arginine to be classified as, **(a)** active or, **(b)** inactive. **(c)** Michaelis-Menten fitting of active members of the library including the WT to estimate kinetic parameters. Data points represent the mean and the error bars the SD (n = 3).

Thermostability test

We measured the melting temperature (T_m) of the WT and variants to estimate the extent to which the change of electrostatic interactions near the active site affected the structural stability of hArg1 (**Figure 4a and 4b**). **Supplementary Table 2** summarizes the melting temperature of the WT and all mutants. The T_m of the WT at pH 7.4 was 80.5 °C in accordance with the previously reported value 81 °C for hArg1.[7] Some variants had a small effect over T_m, with shifts within the range of 3 °C. These mutants also retained their activities best (**Figure 4c**). On the other hand, some variants (E186R, E186K, V145R, V145K, E277D, G18E and G18D) exhibited lower thermostability compared to WT, with T_m values between 7-15 °C lower (**Figure 4b**). Interestingly, all these variants also lost their catalytic function (**Figure 4c** and **Supplementary Table 2**), highlighting the importance of structural and thermal stability in an enzyme's specific activity. All mutations around D128 conferred significantly lower melting temperatures. Since D128 coordinates the Mn^{2+} cofactor, it is likely that the electrostatic interactions from these mutants impacted cofactor coordination and the stability of the catalytic center.

Near H141, the mutation of two residues caused significantly lower T_m values: E277 and G18, which happen to be the closest mutants to H141. E277 forms a hydrogen bond with H141, which is likely broken due to the difference in the side chain length of aspartate and glutamate. We suppose that by mutating G18 we do not only change the electrostatic environment of H141, but due to its proximity, it is also affecting the direction of its side chain in the catalytic center. The significant decrease in thermal stability observed for a subset of charged substitutions indicates that the thermal stability of the enzyme has evolved along its catalytic trajectory.

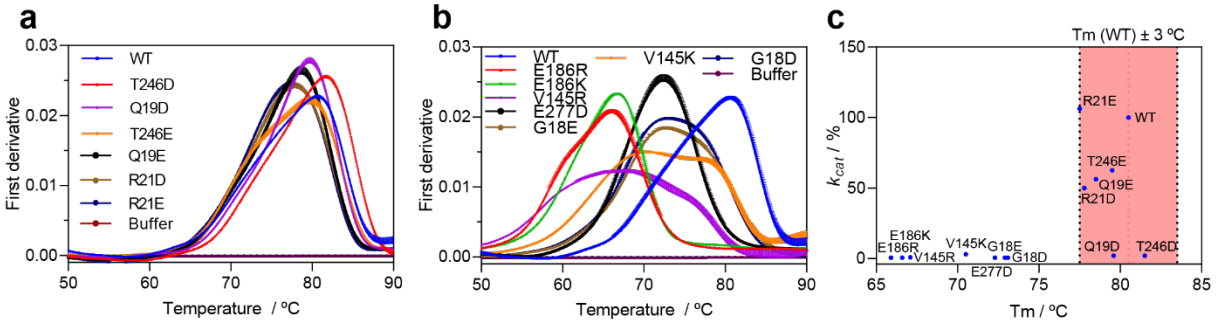

Figure 4. Characterization of thermal stability of WT hArg1 and variants. (a) Differential scanning fluorimetry melting curves of WT and variants with no significant T_m shift. **(b)** Thermal denaturation of variants with destabilized structural folding compared to WT. hArg1 WT and variants were activated by Mn^{2+} at pH 7.4 and measured in triplicates. The T_m of each variant was estimated as the maximum of the first derivative plot. **(c)** Mutants with high destabilization (low T_m) uniformly show little to no activity. Enzymatic activity is shown as a percentage change of k_{cat} over the WT, which was estimated assuming reaction rates were operating at V_{max} conditions at 20 mM L-arginine.

Enzyme display on the surface of *E. coli* for high throughput screening

Our enzyme cascade offers a reliable tool with high specificity and an easy-to-implement workflow. With the advent of DNA synthesis and sequencing, generation of large numbers of genetic variants is no longer a limitation. However, protein synthesis and purification for large libraries would be laborious. To increase the throughput of the assay we worked to display active hArg1 on the cell-surface of *E. coli.* When combined with cell-surface display, variants of an enzyme can be produced at high throughput and the analysis can be performed in parallel as described above. Moreover, since the enzymes are not contained within the biological compartments of the cell, but rather are tethered to the outer membrane, access to substrates and products is not limiting. The lack of control for a specific number of hArg1 molecules on the surface can be a significant limiting factor in enzyme screening, however, with surface display each sample can be normalized to their expression levels, obtained by immunolabeling and flow cytometry. Regardless, a higher background level and lower assay sensitivities are to be expected when operating with whole-cell catalysts.

Specifically, genes encoding a subset of mutant hArg1 sequences were cloned by Gibson assembly in frame with a glycine-serine linker fused to the N-terminus of the autotransporter AIDA-1,[39] a well-established anchor protein, and transformed into the NiCo21 expression E. coli strain. The cells were induced and the expression efficiency was evaluated by immunolabeling and flow cytometry (**Supplementary Figure 6**). The saturating concentration of each auxiliary enzyme was calculated by fixing the cell density and increasing the concentration of each auxiliary enzyme individually (**Supplementary Figure 2d - 2f**). For a cell density of 5 million cells/mL, 1 µM ODC, 500 nM PO and 50 nM HRP were found to be sufficient to make hArg1 rate limiting for the whole cascade. Subsequently, the linearity between cell concentration and reaction rate was determined as before. The assay maintained its linearity within a range of 0 - 7 million cells/mL (**Figure 5b -5c**). Subsequently, a small portion of the library was transferred to the display system, tested and compared to the soluble format of the assay (**Figure 5d**). Since the number of displayed enzyme molecules is not strictly known in absolute terms, k_{cat} cannot be directly quantified. However, if we rank the mutants in order of highest to lowest activity, the order is somewhat maintained (**Figure 5d**) as for the soluble enzymes. This serves as a proof-of-concept for using displayed hArg1 as a pre-screening method that could allow for

much larger libraries to be scanned. In combination with colony pickers and a liquid handling robot, we estimate that a library in the range of 10^3-10^4 members could be screened within one working month, assuming we use a highly optimized method for *E. coli* surface display and screen in 384 microtiter plates. When using higher throughput techniques, such as droplet-based screening or single cell encapsulation, throughput is expected to increase by at least 1 to 2 orders of magnitude.

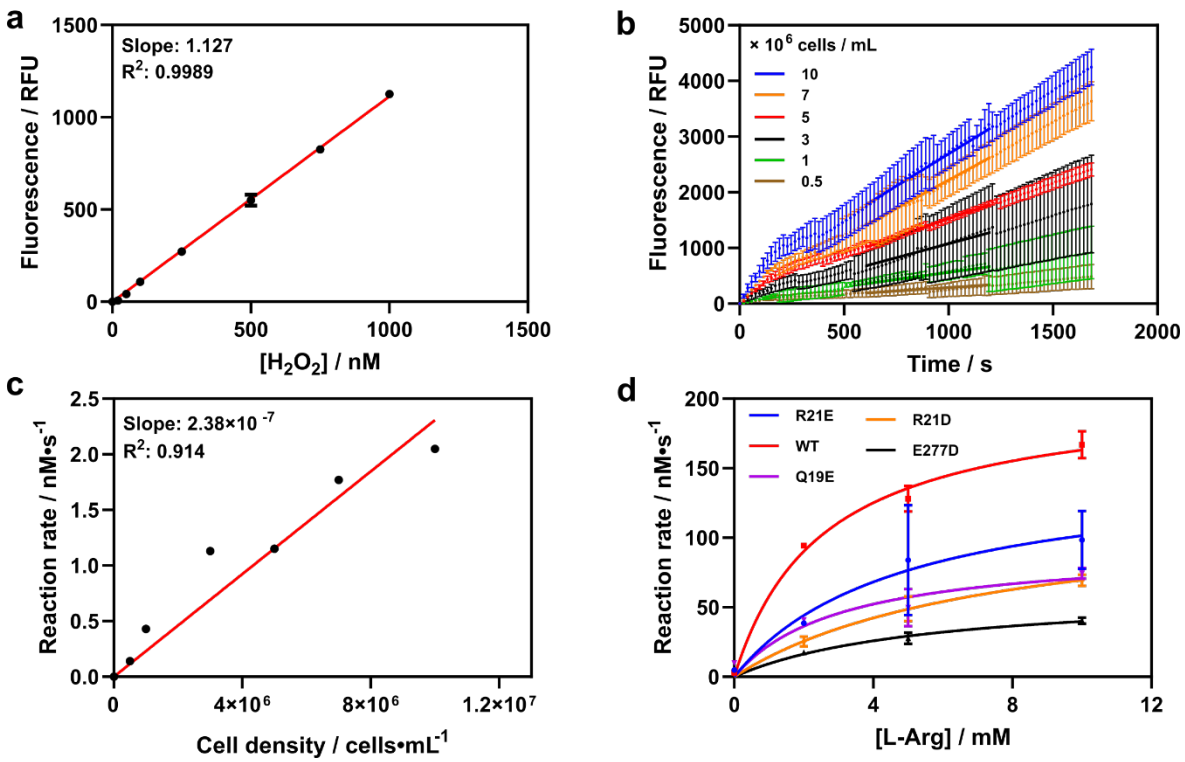

Figure 5: Cell surface display of hArg1 and mutant characterization. (a) Standard curve for Amplex UltraRed in fluorescence mode within 1 µM H_2O_2. **(b)** Time course of a range of hArg1-displaying bacterial cell densities (500,000 to 10 million cells/mL) with 10 mM of L-arginine and the activity assay in fluorescence mode at 37 °C. Data points represent the mean and the error bars the SD (n = 3). The reaction rate was estimated from a linear regression between 600-1200s represented with a solid line. **(c)** The slope of the linear regression in (b) was converted to nM/s with the standard curve (a) and represented for different cell densities to determine the linear range of the assay with displayed cells. **(d)** Michaelis-Menten fitting of $5 \cdot 10^6$ cells/mL of hArg1 WT and a small selection of the library normalized by expression levels to estimate and compare their kinetic parameters.

Conclusion

Given the importance of human arginase as a drug target and therapeutic molecule, there is a clear need for easy-to-implement assay technology that allow exploration of the mutational landscape of arginase as well as its inhibition by small molecules. We presented a novel 4-enzyme cascade that serves as an arginase assay and allows facile study of kinetic and thermodynamic properties of arginase in a simple and reliable manner. The one-pot reaction is based on a peroxidase chemistry, which is not only a well-established reliable method, but also offers flexibility for a wide variety of substrates. Moreover, it can be monitored in real-time allowing us to bypass cumbersome endpoint

measurements. Peroxidase-based systems have been previously reported to be compatible with other currently available high throughput screening methods that are based on labeling with a HRP enzyme, such as single-cell encapsulation[40] or microfluidic-droplet formation[41–43] among others.[44-46] To demonstrate the applicability of the cascade assay, we screened a curated library containing variants with modified electrostatic microenvironments around the hArg1 catalytic center. In this small library, we identified one mutant with slightly improved (13%) turnover number (R21E) as compared with WT. We further combined both thermostability and kinetic activity data to study the how electrostatic changes differentially influenced these parameters. Finally, we combined the cascade assay with cell-surface display of the enzyme to further increase scalability and enable more powerful protein engineering campaigns on arginase. More broadly, this work demonstrates how cascade enzyme systems designed to convert enzyme products into H_2O_2 can leverage advantageous features of peroxidase-compatible screens. Having validated the cell-surface display together with the cascade activity assay, our work will enable analysis of large numbers of arginase variants and/or inhibitor compounds *en route* to therapeutic applications.

Supporting information

Detailed chemicals, materials, protein synthesis and nanoDSF experiments; Kinetic parameters of hArg1 compared to other publications; Kinetic and thermal parameters of hArg1 and library members; Primary amino acid sequences; Size exclusion chromatograms and SDS PAGE analysis for purified proteins; Determination of the concentration of auxiliary enzymes; Characterization of the pH range of the assay; Characterization of hArg1 with the commercial Arginase Activity Assay Kit; Screening of active members of the library; Expression level by mutant and normalization.

Acknowledgements

This work was supported by the University of Basel, ETH Zurich, the SNF NCCR in Molecular Systems Engineering, and an SNSF Grant (200021_191962) to M.A.N. The authors thank the technical support and assistance provided by Joanan López Morales and Florian Seebeck for his help in designing the cascade.

References

(1) Sjöstedt, E.; Zhong, W.; Fagerberg, L.; Karlsson, M.; Mitsios, N.; Adori, C.; Oksvold, P.; Edfors, F.; Limiszewska, A.; Hikmet, F.; Huang, J.; Du, Y.; Lin, L.; Dong, Z.; Yang, L.; Liu, X.; Jiang, H.; Xu, X.; Wang, J.; Yang, H.; Bolund, L.; Mardinoglu, A.; Zhang, C.; von Feilitzen, K.; Lindskog, C.; Pontén, F.; Luo, Y.; Hökfelt, T.; Uhlén, M.; Mulder, J. An Atlas of the Protein-Coding Genes in the Human, Pig, and Mouse Brain. *Science* **2020**, *367* (6482).

(2) Di Costanzo, L.; Sabio, G.; Mora, A.; Rodriguez, P. C.; Ochoa, A. C.; Centeno, F.; Christianson, D. W. Crystal Structure of Human Arginase I at 1.29-Å Resolution and Exploration of Inhibition in the Immune Response. *Proceedings of the National Academy of Sciences* **2005**, *102* (37), 13058–13063.

(3) Di Costanzo, L.; Pique, M. E.; Christianson, D. W. Crystal Structure of Human Arginase I Complexed with Thiosemicarbazide Reveals an Unusual Thiocarbonyl Mu-Sulfide Ligand in the Binuclear Manganese Cluster. *J. Am. Chem. Soc.* **2007**, *129* (20), 6388–6389.

(4) Grobben, Y.; Uitdehaag, J. C. M.; Willemsen-Seegers, N. Structural Insights into Human Arginase-1 pH Dependence and Its Inhibition by the Small Molecule Inhibitor CB-1158. *J. Struct. Biol* **2019**, *2020*.

(5) Clemente, G. S.; van Waarde, A.; F Antunes, I.; Dömling, A.; H Elsinga, P. Arginase as a Potential Biomarker of Disease Progression: A Molecular Imaging Perspective. *Int. J. Mol. Sci.* **2020**, *21* (15).

(6) Yang, Z.; Ming, X.-F. Functions of Arginase Isoforms in Macrophage Inflammatory Responses: Impact on Cardiovascular Diseases and Metabolic Disorders. *Front. Immunol.* **2014**, *5*, 533.

(7) Romero, P. A.; Stone, E.; Lamb, C.; Chantranupong, L.; Krause, A.; Miklos, A. E.; Hughes, R. A.; Fechtel, B.; Ellington, A. D.; Arnold, F. H.; Georgiou, G. SCHEMA-Designed Variants of Human Arginase I and II Reveal Sequence Elements Important to Stability and Catalysis. *ACS Synth. Biol.* **2012**, *1* (6), 221–228.

(8) Stone, E. M.; Chantranupong, L.; Georgiou, G. The Second-Shell Metal Ligands of Human Arginase Affect Coordination of the Nucleophile and Substrate. *Biochemistry* **2010**, *49* (49), 10582–10588.

(9) Rowlinson, S. W.; Alters, S. E.; Agnello, G.; Tyler, J.; Lowe, A.; Okamoto-Kearney, M.; Johnson, D.; Stone, E.; Georgiou, G.; Lowe, D. G. Abstract 1042: Development of AEB1102, an Engineered Human Arginase 1 for Patients with Solid Tumors. *Cancer Res.* **2016**, *76* (14_Supplement), 1042–1042.

(10) Diez-Fernandez, C.; Rüfenacht, V.; Gemperle, C.; Fingerhut, R.; Häberle, J. Mutations and Common Variants in the Human Arginase 1 (ARG1) Gene: Impact on Patients, Diagnostics, and Protein Structure Considerations. *Hum. Mutat.* **2018**, *39* (8), 1029–1050.

(11) Crombez, E. A.; Cederbaum, S. D. Hyperargininemia due to Liver Arginase Deficiency. *Mol. Genet. Metab.* **2005**, *84* (3), 243–251.

(12) Biotherapeutics, A. *A Phase 1/2 Study of AEB1102 in Patients With Arginase I Deficiency*; NCT02488044; 2019. https://clinicaltrials.gov/ct2/show/NCT02488044 (accessed 2022-07-20).

(13) Chan, S. L.; Cheng, P. N. M.; Liu, A. M.; Chan, L. L.; Li, L.; Chu, C. M.; Chong, C. C. N.; Lau, Y. M.; Yeo, W.; Ng, K. K. C.; Yu, S. C. H.; Mok, T. S. K.; Chan, A. W. H. A Phase II Clinical Study on the Efficacy and Predictive Biomarker of Pegylated Recombinant Arginase on Hepatocellular Carcinoma. *Invest. New Drugs* **2021**, *39* (5), 1375–1382.

(14) Tsui, S.-M.; Lam, W.-M.; Lam, T.-L.; Chong, H.-C.; So, P.-K.; Kwok, S.-Y.; Arnold, S.; Cheng, P. N.-M.; Wheatley, D. N.; Lo, W.-H.; Leung, Y.-C. Pegylated Derivatives of Recombinant Human Arginase (rhArg1) for Sustained in Vivo Activity in Cancer Therapy: Preparation, Characterization and Analysis of Their Pharmacodynamics in Vivo and in Vitro and Action upon Hepatocellular Carcinoma Cell (HCC). *Cancer Cell Int.* **2009**, *9*, 9.

(15) Phillips, M. M.; Sheaff, M. T.; Szlosarek, P. W. Targeting Arginine-Dependent Cancers with Arginine-Degrading Enzymes: Opportunities and Challenges. *Cancer Res. Treat.* **2013**, *45* (4), 251–262.

(16) De Santo, C.; Cheng, P.; Beggs, A.; Egan, S.; Bessudo, A.; Mussai, F. Metabolic Therapy with PEG-Arginase Induces a Sustained Complete Remission in Immunotherapy-Resistant Melanoma. *J. Hematol. Oncol.* **2018**, *11* (1), 68.

(17) Stone, E. M.; Glazer, E. S.; Chantranupong, L.; Cherukuri, P.; Breece, R. M.; Tierney, D. L.; Curley, S. A.; Iverson, B. L.; Georgiou, G. Replacing Mn2+ with Co2+ in Human Arginase I Enhances Cytotoxicity toward L-Arginine Auxotrophic Cancer Cell Lines. *ACS Chem. Biol.* **2010**, *5* (3), 333–342.

(18) Jung, D.; Biggs, H.; Erikson, J.; Ledyard, P. U. New Colorimetric Reaction for End-Point, Continuous-Flow, and Kinetic Measurement of Urea. *Clin. Chem.* **1975**, *21* (8), 1136–1140.

(19) Beale, R. N.; Croft, D. A Sensitive Method for the Colorimetric Determination of Urea. *J. Clin. Pathol.* **1961**, *14*, 418–424.

(20) Garganta, C. L.; Bond, J. S. Assay and Kinetics of Arginase. *Analytical Biochemistry* **1986**, *154*, 388–394.

(21) Urbanowicz, M.; Sadowska, K.; Paziewska-Nowak, A.; Sołdatowska, A.; Pijanowska, D. G. Biosensor Based on Coupled Enzyme Reactions for Determination of Arginase Activity. *Bioelectrochemistry* **2022**, *146* (108137), 108137.

(22) Booker, H. E.; Haslam, J. L. Immobilized Enzyme Electrode for the Determination of Arginase. *Anal. Chem.* **1974**, *46* (8), 1054–1060.

(23) Iyamu, E. W.; Asakura, T.; Woods, G. M. A Colorimetric Microplate Assay Method for High-Throughput Analysis of Arginase Activity in Vitro. *Anal. Biochem.* **2008**, *383* (2), 332–334.

(24) Asano, W.; Takahashi, Y.; Kawano, M.; Hantani, Y. Identification of an Arginase II Inhibitor via RapidFire Mass Spectrometry Combined with Hydrophilic Interaction Chromatography. *SLAS Discov* **2019**, *24* (4), 457–465.

(25) Scholle, M. D.; Gurard-Levin, Z. A. Development of a Novel Label-Free and High-Throughput Arginase-1 Assay Using Self-Assembled Monolayer Desorption Ionization Mass Spectrometry. *SLAS Discov* **2021**, 26(6), 775-782.
(26) Grobben, Y.; Willemsen-Seegers, N.; Uitdehaag, J. C. M.; de Man, J.; van Groningen, J.; Friesen, J.; van den Hurk, H.; Buijsman, R. C.; Zaman, G. J. R. High-Throughput Fluorescence-Based Activity Assay for Arginase-1. *SLAS Discov* **2020**, *25* (9), 1018–1025.
(27) *Enzymatic Substrates for ImmunoAssays*; BA357a; Interchim Innovations. https://www.interchim.fr/ft/B/BA357a.pdf.
(28) Benítez-Mateos, A. I.; Roura Padrosa, D.; Paradisi, F. Multistep Enzyme Cascades as a Route towards Green and Sustainable Pharmaceutical Syntheses. *Nat. Chem.* **2022**, *14* (5), 489–499.
(29) Sperl, J. M.; Sieber, V. Multienzyme Cascade Reactions—Status and Recent Advances. *ACS Catal.* **2018**, *8* (3), 2385–2396.
(30) Zhang, Y.; Hess, H. Toward Rational Design of High-Efficiency Enzyme Cascades. *ACS Catal.* **2017**, *7* (9), 6018–6027.
(31) Rosenthal, K.; Bornscheuer, U. T.; Lütz, S. Cascades of Evolved Enzymes for the Synthesis of Complex Molecules. *Angew. Chem. Int. Ed Engl.* **2022**, *61* (39), e202208358.
(32) Finnigan, W.; Hepworth, L. J.; Flitsch, S. L.; Turner, N. J. RetroBioCat as a Computer-Aided Synthesis Planning Tool for Biocatalytic Reactions and Cascades. *Nat Catal* **2021**, *4* (2), 98–104.
(33) Choi, H.; Kyeong, H.-H.; Choi, J. M.; Kim, H.-S. Rational Design of Ornithine Decarboxylase with High Catalytic Activity for the Production of Putrescine. *Appl. Microbiol. Biotechnol.* **2014**, *98* (17), 7483–7490.
(34) Alarcón, R.; Orellana, M. S.; Neira, B.; Uribe, E.; García, J. R.; Carvajal, N. Mutational Analysis of Substrate Recognition by Human Arginase Type I--Agmatinase Activity of the N130D Variant. *FEBS J.* **2006**, *273* (24), 5625–5631.
(35) Tommasi, S.; Elliot, D. J.; Da Boit, M.; Gray, S. R.; Lewis, B. C.; Mangoni, A. A. Homoarginine and Inhibition of Human Arginase Activity: Kinetic Characterization and Biological Relevance. *Sci. Rep.* **2018**, *8* (1).
(36) Ilies, M.; Di Costanzo, L.; Dowling, D. P.; Thorn, K. J.; Christianson, D. W. Binding of α,α-Disubstituted Amino Acids to Arginase Suggests New Avenues for Inhibitor Design. *J. Med. Chem.* **2011**, *54* (15), 5432–5443.
(37) Kanyo, Z. F.; Scolnick, L. R.; Ash, D. E.; Christianson, D. W. Structure of a Unique Binuclear Manganese Cluster in Arginase. *Nature* **1996**, *383* (6600), 554–557.
(38) Carvajal, N.; Olate, J.; Salas, M.; Uribe, E.; López, V.; Herrera, P.; Cerpa, J. Chemical Modification and Site-Directed Mutagenesis of Human Liver Arginase: Evidence That the Imidazole Group of Histidine-141 Is Not Involved in Substrate Binding. *Arch. Biochem. Biophys.* **1999**, *371* (2), 202–206.
(39) Maurer, J.; Jose, J.; Meyer, T. F. Characterization of the Essential Transport Function of the AIDA-I Autotransporter and Evidence Supporting Structural Predictions. *J. Bacteriol.* **1999**, *181* (22), 7014–7020.
(40) Vanella, R.; Bazin, A.; Ta, D. T.; Nash, M. A. Genetically Encoded Stimuli-Responsive Cytoprotective Hydrogel Capsules for Single Cells Provide Novel Genotype–phenotype Linkage. *Chem. Mater.*
(41) Debon, A.; Pott, M.; Obexer, R.; Green, A. P.; Friedrich, L.; Griffiths, A. D.; Hilvert, D. Ultrahigh-Throughput Screening Enables Efficient Single-Round Oxidase Remodelling. *Nature Catalysis* **2019**, *2* (9), 740–747.
(42) Kolaitis, G.; Jain, A.; Romeis, D.; Buryska, T.; Steiger, M.; Wuerstl, L.; Doering, M.; Beer, B.; Stavrakis, S.; deMello, A.; Sieber, V. Development of a Universal NADH Detection Assay for High Throughput Enzyme Evolution Using Fluorescence Activated Droplet Sorting. *ChemRxiv* **2022**.
(43) Obexer, R.; Pott, M.; Zeymer, C.; Griffiths, A. D.; Hilvert, D. Efficient Laboratory Evolution of Computationally Designed Enzymes with Low Starting Activities Using Fluorescence-Activated Droplet Sorting. *Protein Eng. Des. Sel.* **2016**, *29* (9), 355–366.
(44) Vanella, R.; Kovacevic, G.; Doffini, V.; de Santaella, J. F.; Nash, M. High-Throughput Screening, Next Generation Sequencing and Machine Learning: Advanced Methods in Enzyme Engineering. Chem. Commun. 2022
(45) Zeymer, C.; Hilvert, D. Directed Evolution of Protein Catalysts. Annu. Rev. Biochem. 2018, 87, 131–157.
(46) Heinisch, T.; Schwizer, F.; Garabedian, B.; Csibra, E.; Jeschek, M.; Vallapurackal, J.; Pinheiro, V. B.; Marlière, P.; Panke, S.; Ward, T. R. Correction: E. Coli Surface Display of Streptavidin for Directed Evolution of an Allylic Deallylase. Chem. Sci. 2019, 10 (27), 6735.